Structure of random monodisperse foam

Andrew M. Kraynik*
Department 9114 MS0834, Sandia National Laboratories, Albuquerque, New Mexico 87185-0834

Douglas A. Reinelt
Department of Mathematics, Southern Methodist University, Dallas, Texas 75275-0156

Frank van Swol
Department 1834 MS1349, Sandia National Laboratories, Albuquerque, New Mexico 87185-1349
and Department of Chemical and Nuclear Engineering, University of New Mexico, Advanced Materials Laboratory, 1001 University Boulevard SE, Albuquerque, New Mexico 87106

(Received 1 July 2002; published 21 March 2003)

The Surface Evolver was used to calculate the equilibrium microstructure of random monodisperse soap froth, starting from Voronoi partitions of randomly packed spheres. The sphere packing has a strong influence on foam properties, such as E (surface free energy) and $\langle f \rangle$ (average number of faces per cell). This means that random foams composed of equal-volume cells come in a range of structures with different topological and geometric properties. Annealing—subjecting relaxed foams to large-deformation, tension-compression cycles—provokes topological transitions that can further reduce E and $\langle f \rangle$. All of the foams have $\langle f \rangle \leqslant 14$. The topological statistics and census of cell types for fully annealed foams are in excellent agreement with experiments by Matzke. Geometric properties related to surface area, edge length, and stress are evaluated for the foams and their individual cells. Simple models based on regular polygons predict trends for the edge length of individual cells and the area of individual faces. Graphs of surface area vs shape anisotropy for the cells reflect the geometrical frustration in random monodisperse foam, which is epitomized by pentagonal dodecahedra: they have low surface area but do not pack to fill space.

DOI: 10.1103/PhysRevE.67.031403 PACS number(s): 82.70.Rr

I. INTRODUCTION

Matzke's experimental study [1] of bubble shapes in monodisperse foam is a landmark in foam science. In sharp contrast with Kelvin's classic theory [2] on the structure of perfectly ordered foam, Matzke did not find a single Kelvin cell, showed that pentagonal faces were the most common (the Kelvin cell only has quadrilateral and hexagonal faces), and also showed that foams exhibit topological disorder even when all of the cells have the same volume. Kelvin's seminal work has spawned the Kelvin problem [3], which refers to ''the partitioning of three-dimensional space into cells of equal volume and minimum surface area.'' The Weaire-Phelan foam [4] has less surface area than the Kelvin cell, but whether it is the best monodisperse foam remains an open question. (The analogous two-dimensional problem, the honeycomb conjecture, has only recently been proved [5].) In this study, we take a broad view of the Kelvin problem and turn from the idealized world of ordered foams to investigate the cell-level structure of random monodisperse foam through numerical simulation.

''We live in a universe inundated with foam [6].'' This form of soft condensed matter has broad practical application, exhibits fascinating physical phenomena, and poses challenging scientific questions [7–9]. Dry soap foam, commonly referred to as soap froth, is a prototypical random heterogeneous material [10], complex fluid [11], jammed system [12], and geometrically frustrated material [13]. Understanding the structure of foam is prerequisite to predicting properties.

From a geometric point of view, the microstructure of all (liquid and solid) foams is built on a skeleton of polyhedra packed to fill space, and soap froth has the simplest structure of all. In the hypothetical dry limit where liquid volume fraction is zero, thin liquid films degenerate to minimal surfaces that form the faces of polyhedral cells. Under conditions of mechanical equilibrium where the surface free energy is minimized, the local foam geometry obeys Plateau's laws [14,15]: (1) each face has constant mean curvature to balance the pressure difference between adjacent cells; (2) three faces meet at equal dihedral angles of 120° at each cell edge; and (3) four edges join at equal tetrahedral angles of $\cos^{-1}(-1/3) = 109.47°$ at each cell vertex. This local, film-level organization is found in all dry soap foams under static conditions.

The Kelvin cell can be modified to form a different 14-hedron that contains mostly pentagons; the resulting Williams cell [16] has two quadrilaterals, eight pentagons, and four hexagons. Layers of these cells alternate orientation in an ordered foam structure. The Weaire-Phelan foam belongs to a class of crystal structures known as tetrahedrally close packed (TCP) [17], which include the Frank-Kasper phases [18]. Two dozen or so basic TCP structures and countless hybrids [19] contain up to four different polyhedra with 12, 14, 15, or 16 faces. These f-hedra have unique topology: there are 12 pentagonal faces, $f-12$ hexagons, and no two hexagons share an edge. The Weaire-Phelan foam contains

*Electronic address: amkrayn@sandia.gov

two pentagonal dodecahedra and six 14-hedra known as Goldberg polyhedra. The TCP foams have $13\frac{1}{3} \leqslant \langle f \rangle \leqslant 13\frac{1}{2}$, where $\langle f \rangle$ is the average number of faces per cell.

The surface free energy density $E = \sigma S$ is a fundamental property of foams; σ is surface tension and S is surface area per unit volume. The natural scale for E is $\sigma/V^{1/3}$, where V is the cell volume. (V is replaced by the average cell volume in polydisperse foams.) Crude bounds on E are $(36\pi)^{1/3} = 4.8360 < E < 6$, which correspond to a spherical bubble and cubic cell, respectively. It is somewhat surprising that the densest packing of uniform spheres [20] does not lead to an ordered foam structure that is stable. The polyhedron associated with face-centered-cubic (fcc) packing is a rhombic dodecahedron, which violates a topological requirement implied by Plateau's laws: individual foam cells must be trivalent polyhedra (three edges meet at each corner). The ordered foams have lower energy than the rhombic dodecahedron, $E = 3(2^{5/6}) = 5.3454$, and the range of energies is narrow: Weaire-Phelan is the lowest (5.2883) and Sadoc-Mosseri [21] is the highest (5.3421); Kelvin (5.3063) and Williams (5.3371) are in between.

Matzke used a microscope to observe the topology of six hundred cells in the interior of foams that were meticulously assembled—one bubble at a time—with a graduated syringe. Matzke reported that $\langle f \rangle = 13.70$, which is in between TCP foams and the Kelvin cell. The cells were grouped according to their face content and labeled n_4-n_5-n_6(n_7), where n_i is the number of faces with i edges. This classification scheme does not distinguish between the different topological permutations that are possible. For example, the faces in trivalent 14-hedra designated as 2-8-4 can be assembled to form eleven topologically distinct polyhedra [22], which include the Williams cell mentioned above. There are even three different ways to make 6-0-8; the Kelvin cell is the most symmetric.

Most of Matzke's ''central'' bubbles had 12 to 16 faces; 11 and 17 were rare. Most of the faces had 4 to 6 edges; trianglular faces were absent and heptagons were rare. Thirty six combinations of faces were found. Bubbles with 14 faces were most common but the most abundant combination (19.7%) was the 13-hedron, 1-10-2, which can only be made one way. We propose calling this unique polyhedron the Matzke cell. Matzke concluded that no single combination could be considered typical because four types were required to form the majority of bubbles and the ten most common types only covered about 80% of his sample. The cell types n_4-n_5-n_6 satisfy

$$n_5 = 12 - 2n_4, \tag{1}$$

$$n_6 = f + n_4 - 12.$$

This pattern and the prevalence of pentagons led Matzke to comment on the absence of three cells: 1-10-0, 1-10-1, and 0-12-1. It is now known that trivalent polyhedra with these combinations of faces do not exist [23]. Consequently, 33 combinations that satisfy Eq. (1), $0 \leqslant n_4 \leqslant 6$ and $12 \leqslant f \leqslant 16$ are possible; Matzke found 23 of them.

Monnereau *et al.* [24] used optical tomography to investigate the topology and coarsening of slightly polydisperse foam, prepared by bubbling nitrogen into surfactant solutions. Cell volumes were calculated from Surface Evolver [25] models of reconstructed foam. The cell statistics were consistent with Matzke, but the samples were smaller. It is noteworthy that the foam topology did not change during the first several hours of an experiment. Matzke's foams were probably even more stable against gas diffusion because his soap solutions contained higher concentrations of glycerine, and therefore were more viscous and had lower gas permeability.

In the current study, random foams are modeled as spatially periodic structures, but unlike the ordered systems, the representative volume (unit cell) contains a large number of bubbles jammed together in a disordered packing. The cells are constrained to have equal volumes so these systems lack volumetric disorder but do possess other characteristics of real foam. These include topological disorder and statistical variation in geometric properties related to cell area and edge length. Consequently, the monodisperse limit is quite rich and provides a baseline for the broader study of polydisperse foam [26].

Real soap froth is notoriously fragile, far from equilibrium, and subject to well-known degradation mechanisms such as coarsening, drainage, and film rupture. Matzke's discussion of experimental technique inspires confidence that uncertainties were controlled, but his study has never been repeated. These uncertainties do not exist in our simulations. The methods used to generate random microstructure are well defined: initial conditions for Surface Evolver simulations are based on Voronoi tessellations, which in turn are based on random packings of identical spheres. Equal cell volumes are set very accurately during relaxation. There is no gas diffusion to cause coarsening and no liquid to drain. There are no boundaries to cause edge effects, i.e., there are no ''peripheral'' cells only ''central'' cells in spatially periodic systems, which represent bulk foam. We consider the simulations to be a critical test of Matzke's experiments and find that our results are in remarkable agreement with his observations.

II. THEORY AND SIMULATIONS

The basic strategy for developing spatially periodic models of random foam in three dimensions carries over from two dimensions [27], and involves two steps: (1) filling space (the plane) with Voronoi polyhedra (polygons) produced from random packings of monodisperse spheres (disks) and (2) relaxing the Voronoi structures to satisfy Plateau's laws and minimize surface area (edge length). The microstructures contain N spheres, convex polyhedra, or bubbles, packed in cubic unit cells.

Recall that a Voronoi cell is defined as a region composed of points that are closer to a given seed point (sphere center) than any other, and the faces are flat. Voronoi foams satisfy the topological requirements on edge and face connectivity in Plateau's laws but not the geometric conditions; e.g., the vertex angles of a flat face with straight edges cannot all be

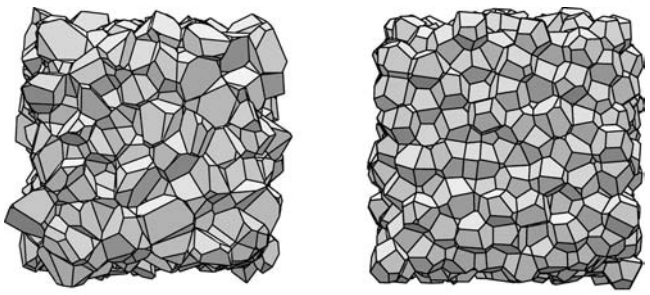

FIG. 1. The first Voronoi structure (V512-RSA) is based on a relatively loose packing of 512 spheres ($\phi=0.36$) produced by random sequential adsorption; the other (V512-RCP) is based on random close packing ($\phi=0.64$) accomplished by molecular dynamics.

equal to the tetrahedral angle. Voronoi cells do not have equal volumes. Polydispersity and other geometric properties of Voronoi tessellations are controlled by setting ϕ, the density of spheres, in various packing algorithms [28,29]. The dispersion of the cell volumes decreases as ϕ increases.

Two methods for packing hard spheres are used in this study: (1) random sequential adsorption (RSA), which produces relatively loose packings, and (2) classical hard-sphere molecular dynamics, which is used to obtain higher densities such as random close packing (RCP), where $\phi=0.64$. RSA is a very simple process. Spheres are randomly, sequentially, and irreversibly deposited in the unit cell unless they overlap. The saturation limit for RSA is $\phi\approx 0.38$. Voronoi foams based on RSA can achieve cell volume dispersions as low as $\sigma_V=0.12$ near saturation; σ_V is the standard deviation. Molecular dynamics can produce much lower dispersion: $\sigma_V=0.042$ at RCP. Sullivan's VCS software [30,31] was used to generate Voronoi partitions. The structures shown in Fig. 1 illustrate the strong influence of ϕ on the regularity of Voronoi cells. Future reference to RSA will indicate sphere packings with $\phi\approx 0.36$; lower density increases irregularity, but has negligible effect on foam properties when the cells are constrained to have equal volumes during relaxation. The resulting foams are monodisperse even though the Voronoi structures are not.

The numerical procedure for relaxing Voronoi structures to produce stable foams is based on the Surface Evolver [25], a computer program that converges to a local minimum by simulating the process of evolution by mean curvature [32]. The Surface Evolver has become the standard computer software for calculating minimal surfaces in foams [33]. The Evolver implements a finite element method that is capable of solving a broad range of problems involving surfaces shaped by energy minimization. The program has many features that enable the simulation of random foams, e.g., the ability to handle complex topology, a hallmark of real soap froth.

Surface Evolver models use triangular facets to discretize the foam structure. The initial datafile produces an unrefined mesh with well-defined characteristics: each n-sided face (with more than three edges) is subdivided into n linear (flat) triangular facets that share a common vertex in the interior of the face. This mesh will be referred to as $\mathcal{R}0$-linear, i.e., zeroth level of refinement and linear facets. Mesh refinement involves subdividing each facet into four similar triangles, so $\mathcal{R}i$ has 4^i times as many facets as $\mathcal{R}0$. Hundreds of simulations indicate that the basic mesh, $\mathcal{R}0$-linear, is adequate for computing the stable structure of random monodisperse foams that contain a large number of cells ($N=216$ and 512). The supporting evidence is discussed below. Calculations involving finer meshes, higher order facets, and up to 1000 cells will also be discussed.

The primary criterion used to establish the stability of a foam structure is based on the length of individual cell edges. All of the edges in a stable foam have finite length as the surface converges to minimum area. Short edges that violate this condition are identified by: $\lambda<\epsilon\langle\lambda\rangle$, where λ is the edge length, $\langle\lambda\rangle$ is the average, and $0.01\leqslant\epsilon\leqslant 0.10$ (0.05 is typical).

In sharp contrast to monodisperse foams (real or ideal), Voronoi polyhedra generated from randomly packed spheres contain many small triangular faces that are virtually eliminated by topological transitions [34,35] during foam relaxation. The main feature of the relaxation algorithm is a loop that terminates when convergence criteria are satisfied and stability is achieved. The loop contains three basic steps: (1) surface evolution, (2) topological transitions, and (3) mesh cleanup. The surface evolves toward minimum energy by taking hundreds of conjugate-gradient iteration steps. The motion stalls when cell edges shrink to zero length and produce skinny triangles. This situation is signaled by a scale factor for the motion dropping below some threshold. Topological transitions are triggered by deleting short cell edges. This produces locally unstable conditions because more than four edges meet at a vertex, or, more than three faces meet at an edge. Local stability is restored by using standard Surface Evolver commands that remove nonminimal features, i.e., ''pop nonminimal edges'' and ''pop nonminimal vertices.'' This process causes cell-neighbor switching [9,36]. The pop commands produce a lot of extra facets in the neighborhood of the unstable features. Mesh cleanup restores the surface to the standard mesh, $\mathcal{R}0$-linear, by deleting extraneous facets.

Random Voronoi foams also contain many short edges that continue to shrink as the surface evolves. The first pass through the relaxation loop causes about $0.1N$ local topology changes; the last few cycles may only involve one or two transitions. Successful simulations converge after a few dozen cycles. Occasionally, the relaxation process fails to converge; short cell edges cannot be eliminated permanently because the pop commands do not produce new cell neighbors. This is apparently caused by using $\mathcal{R}0$-linear; the local geometry is a poor approximation of the curved features on minimal surfaces. We have found that using finer meshes or higher order (quadratic) facets always causes the shortest edge length λ_{min} to increase. Consequently, most simulations that do not converge with $\mathcal{R}0$-linear, do converge when the calculations are performed with highly refined meshes and higher order facets. Furthermore, every simulation that converges with $\mathcal{R}0$-linear, also converges with mesh refinement. This supports the following conjecture: convergence with $\mathcal{R}0$-linear guarantees foam stability. These calculations are conservative and less demanding on computer resources. The

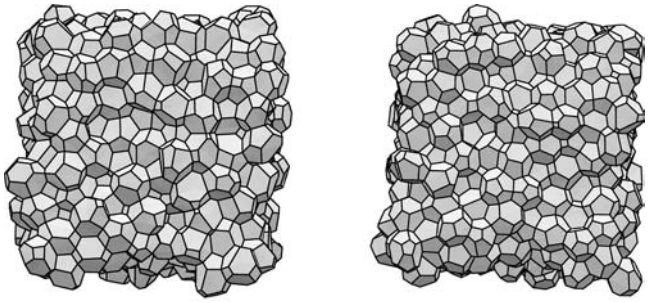

FIG. 2. The first random monodisperse foam (R512-RSA) was annealed to produce the second (RA512-RSA). It is not obvious that they have significantly different properties (see Table I). The corresponding initial condition (V512-RSA) is shown in Fig. 1.

distribution of edge lengths in relaxed foams is sufficiently narrow that λ_{min} is often well above the cut off; i.e., $\lambda_{min} \approx 0.25\langle\lambda\rangle$.

The Voronoi tessellation associated with a particular packing of spheres is unique. In contrast, the detailed geometry and topology of foams produced from a particular Voronoi structure depend on a number of adjustable parameters that control relaxation. These parameters include thresholds that define short edges and stalling, the number of iterations at various stages of the process, etc. However, the global properties of relaxed monodisperse foam, such as E and $\langle f\rangle$, are insensitive to the control parameters used.

Convergence issues and the strong influence of packing density on foam properties motivated us to develop a systematic method for perturbing foams to alter the microstructure. This was accomplished by mechanical *annealing*–subjecting fully relaxed structures to large homogeneous deformations followed by relaxation. The process exploits the well-known elastic-plastic behavior of soap froth, which is caused by shear-induced structural rearrangements [3,36–40]. The annealing algorithm involves large-deformation tension-compression cycles repeated along the three axes of the cubic unit cell. Each cycle is composed of four successive step strains of magnitude 6/5, 5/6, 5/6, and 6/5. The strains are large enough to provoke a lot of cell-neighbor switching, but small enough to prevent the buildup of residual stress that is associated with hysteresis in elastic-plastic systems. Figure 2 shows a typical foam before and after annealing.

The effective macroscopic stress σ_{ij} of a dry soap foam is calculated by averaging the local position-dependent stress over the unit cell [41]:

$$\sigma_{ij} = -\frac{1}{NV}\sum_{k=1}^{N}(p_k V_k)\,\delta_{ij} + \frac{2\sigma}{NV}\int_{\mathcal{S}}(\delta_{ij} - n_i n_j)\,ds. \quad (2)$$

Here, p_k and V_k are the pressure and volume of individual bubbles that are partitioned by surface $\mathcal{S}$; δ_{ij} is the Kronecker delta; n_i is a local unit vector normal to surface $\mathcal{S}$; and ds is the differential area element. The factor of 2 occurs because each surface (soap film) has two sides. For monodisperse foam $V_k = V$. All of the nonisotropic contributions to the stress come from the surface integral.

In general, the stress is not isotropic for random foams that are confined to cubic unit cells. This is relevant because relieving the excess stress reduces the energy. The foam experiences elastic recoil, which distorts the cubic unit cell into a parallelepiped with three different edge lengths and no right angles. The small corrections to E that result from relaxing the lattice to achieve isotropic stress will be discussed in Sec. III.

TABLE I. Global topological and geometric properties of various foam structures, and, a census of cell types. E is scaled by $\sigma/V^{1/3}$ and L, the total cell edge length per unit volume of foam, is scaled by $V^{-2/3}$. The fourteen most common types found by Matzke are included.

Cell Type	$\langle S_k\rangle$	Matzke	RA512 RSA	RA216 RSA	RA512 RCP	RA216 RCP	R512 RCP	R512 RSA	V1000 RCP	V1000 RSA	R216 X	R864 FCC
$\langle f\rangle$		13.70	13.71	13.69	13.74	13.74	13.85	13.94	14.28	14.90	14.00	14.00
E			5.328	5.331	5.326	5.327	5.339	5.371	5.398	5.539	5.334	5.326
L			5.390	5.393	5.388	5.388	5.403	5.436	5.462	5.580	5.399	5.393
μ_2		1.066	0.995	1.214	0.879	0.812	1.025	1.460	1.360	3.089	0.500	0.336
0-12-0	5.291	8.3%	8.0	10.6	6.1	6.5	3.4	1.1	1.1	0.0	0.0	0.0
2-8-2	5.313	2.5	2.6	2.8	2.0	1.0	3.6	3.6	1.7	0.5	0.0	0.0
1-10-2	5.314	19.7	20.3	18.8	18.5	20.0	10.4	5.7	3.3	0.3	0.0	0.1
2-8-3	5.333	3.2	2.5	3.5	2.8	2.6	4.1	4.3	2.0	0.2	0.0	0.0
3-6-4	5.329	6.0	5.4	5.1	7.2	8.1	10.2	8.9	5.9	1.2	9.7	3.1
0-12-2	5.316	6.5	8.4	8.7	7.6	6.9	1.9	1.5	0.2	0.0	0.0	0.0
1-10-3	5.331	12.2	9.5	12.2	11.2	11.1	6.2	4.0	1.6	0.1	0.0	0.0
2-8-4	5.336	10.7	13.9	9.6	14.5	17.1	13.4	9.3	5.0	0.6	0.5	1.7
3-6-5	5.354	2.8	2.9	3.1	5.3	4.0	9.0	6.4	4.6	0.6	6.5	6.1
4-4-6	5.350	2.0	1.9	1.0	2.4	1.2	5.2	3.5	3.5	0.5	48.6	36.9
0-12-3	5.321	3.5	5.2	3.9	2.6	2.8	1.0	1.0	0.1	0.0	0.0	0.0
1-10-4	5.337	5.8	6.0	6.4	4.6	5.5	3.9	3.3	0.7	0.1	0.5	0.0
2-8-5	5.349	4.0	3.5	2.9	5.0	3.1	5.3	4.2	1.8	0.3	0.9	0.0
0-12-4	5.329	1.7	1.0	2.0	1.3	1.4	0.5	0.4	0.0	0.0	0.0	0.0

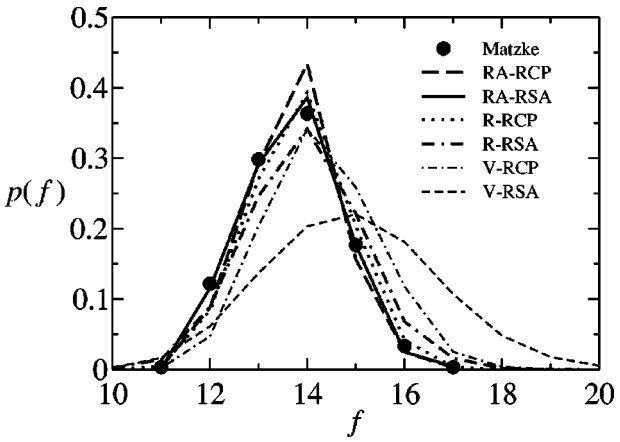

FIG. 3. Distribution of cells with f faces.

The deviatoric stress σ'_{ij} is the nonisotropic part of σ_{ij} [42]. The scalar Σ, the magnitude of σ'_{ij}, is given by

$$\Sigma = (J_2)^{1/2} = \left(\frac{1}{2}\sigma'_{ij}\sigma'_{ij}\right)^{1/2}, \tag{3}$$

$$\sigma'_{ij} = \sigma_{ij} - \frac{1}{3}\sigma_{ll}\delta_{ij} = \frac{2\sigma}{NV}\int_{\mathcal{S}}\left(\frac{1}{3}\delta_{ij} - n_i n_j\right)ds$$

$$= \frac{\sigma}{NV}\sum_{k=1}^{N}\int_{\mathcal{S}_k}\left(\frac{1}{3}\delta_{ij} - n_i n_j\right)ds,$$

where J_2 is a scalar tensor invariant, and $\mathcal{S}_k$ is the surface of individual bubbles. The quantity Σ is a measure of stress anisotropy for the entire foam. We introduce an analogous measure for the shape anisotropy of individual foam cells: the scalar Q_k is defined by

$$Q_k = \left(\frac{1}{2}q^k{}_{ij}q^k{}_{ij}\right)^{1/2}, \tag{4}$$

$$q^k{}_{ij} = {V_k}^{-2/3}\int_{\mathcal{S}_k}\left(\frac{1}{3}\delta_{ij} - n_i n_j\right)ds.$$

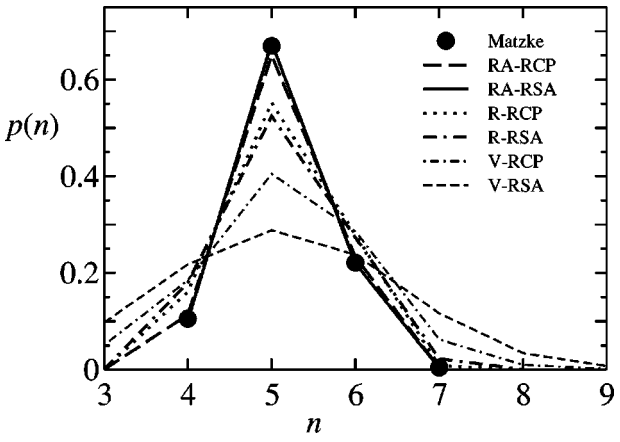

FIG. 4. Distribution of faces with n edges.

The integral is evaluated over the surface of individual bubbles, which distinguishes $q^k{}_{ij}$ from the interface tensor that appears in the Doi-Ohta theory for the rheology of complex interfaces [43]. By comparing Eqs. (2)–(4) it is clear that $q^k{}_{ij}$ can be viewed as the ''bubble interface stress.'' The components of $q^k{}_{ij}$ and the scalar Q_k are zero for highly symmetric objects such as spheres, cubes, and regular dodecahedra.

III. RESULTS AND DISCUSSION

The following scheme is used in the text and figures to distinguish between various foam structures: V (Voronoi), R (relaxed), or RA (relaxed and annealed), followed by the system size (N) and sphere-packing conditions. For example, R512-RCP refers to a relaxed foam that contains 512 cells; the initial condition was built from random close packed spheres. RSA refers to loose sphere packings with $\phi \approx 0.36$ generated by random sequential adsorption. Table I contains data on the global foam properties E, $\langle f\rangle$, and μ_2. All quantities are dimensionless; energy and stress are scaled by $\sigma/V^{1/3}$ and length is scaled by $V^{1/3}$. The variance of f, defined by

$$\mu_2 = \langle f^2\rangle - \langle f\rangle^2, \tag{5}$$

is a measure of topological disorder. It is unnecessary to report the average number of edges per face $\langle n\rangle$ because this quantity is related to $\langle f\rangle$ through

$$\langle f\rangle = \frac{12}{6 - \langle n\rangle}. \tag{6}$$

This identity is derived from Euler's equation and applies to spatially periodic systems that have the connectivity of soap froth. Surface areas and other metrics of foam structure are calculated using $\mathcal{R}0$-quadratic, unrefined meshes and quadratic facets. Convergence studies using highly refined quadratic meshes ($\mathcal{R}2$-quadratic) indicate that E is accurate to within 0.001% when $\mathcal{R}0$-quadratic is used. The probability $p(f)$ that a cell has f faces, and $p(n)$ that a face has n edges, is graphed in Figs. 3 and 4.

Results for the Voronoi structures shown in Table I are based on averages of ten samples. All of the Voronoi foams have $\langle f\rangle > 14$. All of the fully relaxed monodisperse foams have $\langle f\rangle \leqslant 14$. The Voronoi structures based on RSA (V-RSA) have the largest values of $\langle f\rangle = 14.90$ and $\mu_2 = 3.09$, and the largest surface area, $E = 5.54$, which shows how far they are from equilibrium. Ongoing studies indicate that polydisperse foams have lower E and $\langle f\rangle$ than monodisperse foams. Consequently, V-RSA structures would be even farther from equilibrium if the original cell volumes were used as constraints in the Surface Evolver calculations.

Results for R512-RSA and R512-RCP refer to relaxed foams built from 20 V-RSA and 30 V-RCP structures, respectively. Data for R216 and R1000 are not presented but are similar. The difference between R-RSA and R-RCP foams, as measured by E and $\langle f\rangle$, is striking (see Table I and Fig. 5). The V-RSA foams, which initially have higher surface area than the V-RCP foams, settle into higher local minima during

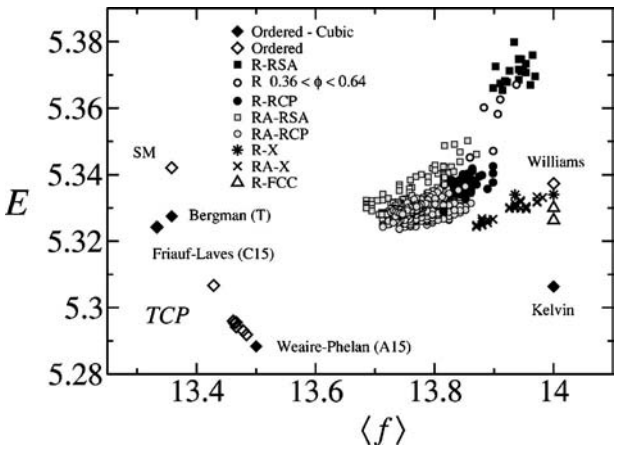

FIG. 5. E vs $\langle f \rangle$ for various relaxed monodisperse foams. All of the figures involve dimensionless quantities; energy and stress are scaled by $\sigma/V^{1/3}$ and length is scaled by $V^{1/3}$.

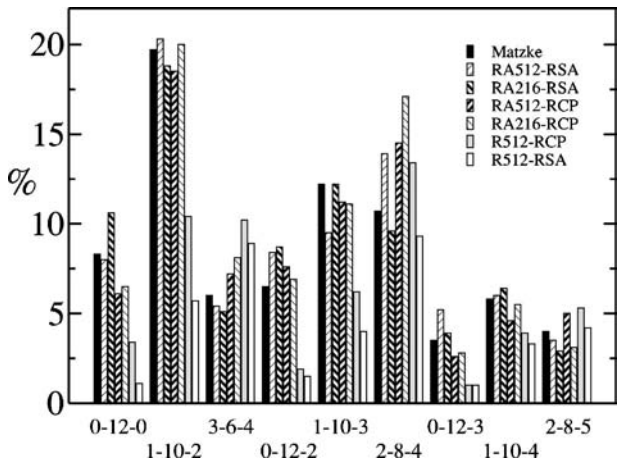

FIG. 6. Cell population in various random monodisperse foams. The annealed foams (RA) are in excellent agreement with Matzke's data. The foam that was produced from a loose sphere packing and not annealed (R512-RSA) is quite different from the others.

the relaxation process. Molecular dynamics was used to pack spheres in the density range $0.36 < \phi < 0.64$ to produce relaxed structures with properties that are in between R-RSA and R-RCP foams. This suggests that the corresponding intermediate region in Fig. 5 is covered by random monodisperse foams.

Several relaxed foams were annealed until they reached a stationary state based on E and $\langle f \rangle$. The results are presented in Table I. In one case, a specific structure (R512-RSA) was subjected to 14 tension-compression cycles in three different directions. Data for the last 15 of 42 structures were averaged to obtain the (stationary) properties designated RA512-RSA. This particular simulation required more than two weeks of CPU time on a workstation. The f and n distributions for fully annealed foams are in excellent agreement with Matzke (see Figs. 3 and 4). Notice how the peak in pentagonal faces builds as the structures are relaxed and then annealed.

The results presented in Fig. 5 show that random monodisperse foams fall within a well-defined region in E-$\langle f \rangle$ space. The corresponding limits, $5.324 \leqslant E \leqslant 5.380$ and $13.68 \leqslant \langle f \rangle \leqslant 13.97$, suggest that a range of microstructures is involved. The simulations are consistent with experiment on the basis of $\langle f \rangle$ since Matzke measured $\langle f \rangle = 13.70$. The annealing process drives random monodisperse foams toward stationary states with lower $E = 5.330 \pm 0.006$ and $\langle f \rangle = 13.74 \pm 0.06$.

Table I also contains a census of cell types. The results are based on several hundred foam structures that contain hundreds of cells. Matzke's sample size was 600 cells. Less than 5% of the cells in V-RSA structures are represented in the table, as opposed to 31% for the V-RCP structures. Consistent with every basis for comparison used in this study, Voronoi structures based on RSA are the least foamlike. Recall that there are 33 types of cells with $12 \leqslant f \leqslant 16$ and $4 \leqslant n \leqslant 6$. We found all 28 types that contain pentagons. Of the remaining five (6-0-n_6) only the Kelvin cell was present in relaxed monodisperse foams; 6-0-6 and 6-0-7 were detected in Voronoi structures. Kelvin cells are rare but this is not surprising since pentagonal faces are so abundant and the Kelvin cell has none. Relaxed foams are much closer to Matzke's results than Voronoi foams; and relaxed foams based on RCP are closer than those based on RSA. Matzke did not find any cells with more than one heptagonal face; the 14-hedron 3-7-3-1 was the most common cell with any. The R-RSA foams, in particular, contain cells with two or even three heptagons (e.g., 6-2-3-2, 3-8-1-2, 5-5-1-3, and 4-7-3-3), cells with octagons (5-4-5-0-1), and cells with both (5-6-2-2-1). The relaxation process eliminates virtually all triangular faces, which are prevalent in Voronoi structures but absent in the experiments. On rare occasions triangular faces do survive relaxation and we have verified that they are stable under mesh refinement. They obviously occur on tetrahedral cells in real foams that are highly polydisperse, and there is no reason to believe that triangular faces cannot exist in monodisperse foam.

The cell inventories for the fully annealed foams are in remarkable agreement with experiment, as shown in Fig. 6. The Matzke cell, 1-10-2, is the most abundant, followed by the 14-hedra: 1-10-3 and 2-8-4. The pentagonal dodecahedron, the prototypical foam cell, is also common. Annealing causes the populations of 0-12-0, 1-10-2, 0-12-2, and 1-10-3 to increase substantially; coincidentally, these cells all have unique topology.

The conditions in the molecular dynamics simulations are controlled to produce random sphere packings, but occasionally the system begins to crystallize [44]. This occurred in two simulations with 216 spheres and has a strong influence on the microstructure of relaxed foams. The effect on E and $\langle f \rangle$ is shown in Fig. 5; foams labeled R-X and RA-X (X for crystalline) fall outside the range that corresponds to random monodisperse foam. One structure (R216-X) has $\langle f \rangle = 14$. The difference in cell inventory between it and the random foams is striking (see Table I). The most common cells in the latter are absent from R216-X, which contains 48.6% 4-4-6 and 6.5% Kelvin cells. Similar behavior was observed by sightly perturbing an fcc packing of spheres ($\phi \approx 0.73$) and producing other relaxed foams that have $\langle f \rangle = 14$. One such structure (R864-FCC) contained 23.4% Kelvin cells, 8.1%

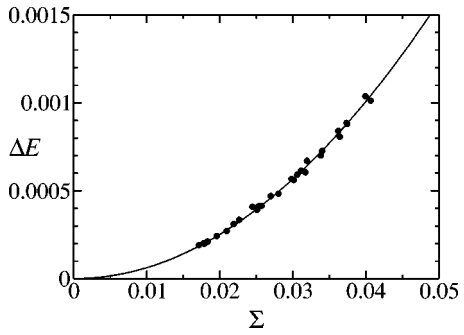

FIG. 7. Reduction in surface free energy ΔE that results from relaxing the lattice to achieve isotropic stress ($\Sigma \approx 0$). The curve refers to Eq. (7) with $G=0.82$.

5-2-6, 7.1% 4-4-7, and 6.6% 5-2-8; none of these cells is included in the tabulated results. We consider these foam structures to be atypical and artifacts of the initial conditions. Annealing did not convert them into random foams, but exhaustive studies were not pursued.

The energies reported in Table I and Fig. 5 have been corrected for foam anisotropy. The adjustments are based on the assumption that random monodisperse foams exhibit isotropic linear elastic behavior. The change in energy ΔE is given by [45]

$$\Delta E = \frac{1}{2} G \gamma^2 = \frac{1}{2G} \Sigma^2, \tag{7}$$

where G is the shear modulus and γ is strain. The lattice vectors for R216 foams were adjusted until isotropic stress was achieved, i.e., $\Sigma \approx 0$. The results for ΔE graphed against Σ are compared with Eq. (7) in Fig. 7. The shear modulus $G=0.82\sigma/V^{1/3}$ measured by Princen and Kiss [46,47] was used in the comparison; regression analysis gave $G=0.79$. Excellent agreement between the simulations and theory supports the use of Eq. (7) to correct for foam anisotropy, and shows that the simulations are consistent with experimental measurements of the shear modulus. Since Σ and the corresponding strains are around 5%, it is reasonable to assume that linear elasticity applies. The energy corrections for foam anisotropy are small (~ 0.001).

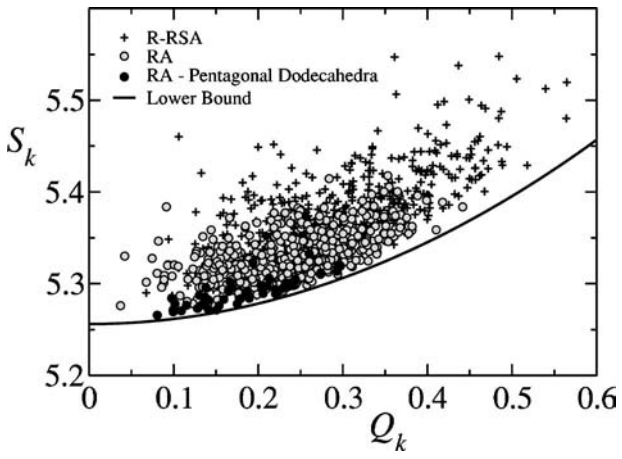

FIG. 8. Surface area S_k vs shape anisotropy Q_k for each cell in a foam before (R512-RSA) and after (RA512-RSA) it is fully annealed. The lower bound refers to Eq. (8).

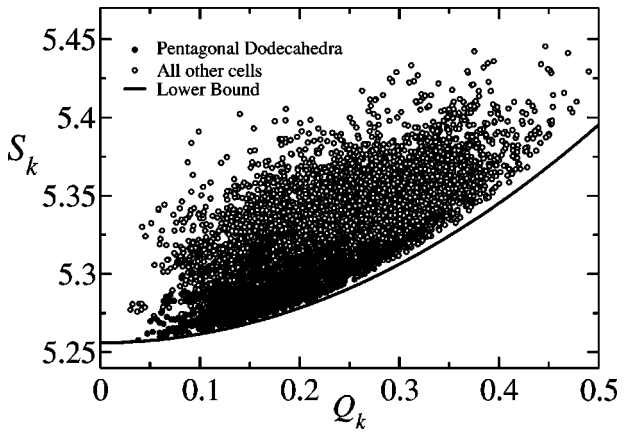

FIG. 9. Surface area S_k vs shape anisotropy Q_k for cells in fully annealed foams.

The surface area S_k and shape anisotropy Q_k are useful geometric characteristics of individual foam cells. A graph of S_k vs Q_k for each cell in a particular foam structure, before (R512-RSA) and after (RA512-RSA) annealing, is presented in Fig. 8. In general, the cells in R-RSA foams are more irregular and many of them have larger surface area and shape anisotropy than the cells in other foams. The S_k-Q_k region has a sharp lower boundary. We have found that a simple quadratic relation given by

$$S = S_{12} + \frac{1}{2G_{12}} Q^2, \tag{8}$$

provides a lower bound on S_k-Q_k data. The parameter $S_{12}=5.2560$ is the surface area of a *minimal regular dodecahedron*. This object is very symmetric: the cell edges have equal length, and the surrounding bubbles are identical and have lower pressure. The other parameter $G_{12}=0.8969$ can be viewed as the ''shear modulus'' for pentagonal dodecahedra, by analogy with Eq. (7). The value of G_{12} was fixed by considering the dodecahedra contained in the Friauf-Laves foam, a TCP structure also known as C15 [17]. These dodecahedra are highly anisotropic ($S_k=5.3451$, $Q_k=0.3997$). The observation that pentagonal dodecahedra are clustered near the bottom of S_k-Q_k graphs inspired us to focus on this cell (see Figs. 8 and 9). The average surface area $\langle S_k \rangle$ for each cell type is presented in Table I; pentagonal dodecahedra (5.291) are lower than all others (5.314–5.354). The minimal regular dodecahedron has lower surface area than any cell in the foams that were examined; however, it does not provide a strict lower bound. Brakke [48] recently used spherical inversion, a conformal transformation, to show that the minimal regular dodecahedron is a saddle point; the transformation to a sphere involves monotonic decrease of the surface-to-volume ratio. The corresponding objects are consistent with Plateau's laws.

The quantity Σ is a global (foam-level) measure of anisotropy and Q_k is a local (cell-level) measure. Since G and G_{12}

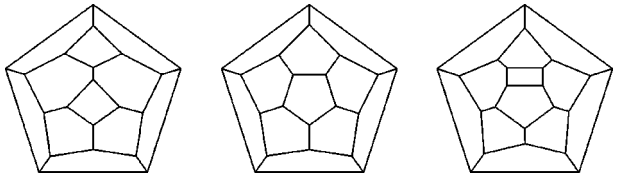

FIG. 10. Schlegel diagrams of three polyhedra: 2-8-2, pentagonal dodecahedron (0-12-0), and Matzke cell (1-10-2). Consider topological transitions that involve the horizontal edge on the central pentagon on 0-12-0. Switching this edge (performing a T1) gives 2-8-2. Splitting this edge (inserting a quadrilateral face) gives 1-10-2.

are both near unity, the magnitudes of Σ and Q_k can be directly compared and viewed as measures of stress or strain. Figure 9 contains an S_k-Q_k graph for several thousand cells in fully annealed (RA) foams. The graph illustrates geometrical frustration in foams. Cells are scarce in the immediate vicinity of the minimal dodecahedron. Pentagonal dodecahedra cannot pack to fill space. Packing in monodisperse foams requires more neighbors on average than twelve: a minimum of $13\frac{1}{3}$ in TCP foams (C15) and around 13.75 in random foams. The magnitude of Q_k (with an average value of 0.233 ± 0.071) indicates that most cells are quite distorted when jammed together.

We can gain insight into the types of cells found in random monodisperse foam by analyzing topological transitions [9,34–36] and focusing on the central role of pentagonal dodecahedra. We will not consider rearrangements that involve cells with triangular faces because they are scarce in monodisperse foam, and for similar reasons, we will not consider cells with fewer than twelve faces. This leaves us with two basic topology changes for the pentagonal dodecahedron and both are illustrated in Fig. 10 with the aid of Schlegel diagrams. There are only two possibilities because every edge is topologically equivalent. In the first case, edge switching (reminiscent of a T1 in two dimensions) rearranges the faces to form a different 12-hedron, 2-8-2. The second case involves edge splitting, whereby a quadrilateral face is inserted at an edge, and results in 1-10-2. The latter indicates why Matzke cells are so common—they aspire to become pentagonal dodecahedra by losing a quadrilateral face through the reverse topology change.

Topological transitions that involve Matzke cells are equally illuminating. There are more possibilities because the edges on 1-10-2 are not all topologically equivalent so we will just summarize the results. There are 33 ways to switch edges: 11 result in 3-6-4; 6 result in 2-8-3; and 4 give back 1-10-2. This indicates why 3-6-4 may be more common than 2-8-3 even though the latter has more pentagonal faces. The other 12 ways of switching edges produce 13-hedra with triangular or heptagonal faces. There are also 33 ways to add quadrilateral faces to a Matzke cell: 19 produce various forms of 2-8-4; 4 result in 1-10-3; and the other ten possibilities lead to heptagonal faces. The fact that 1-10-2 and 2-8-4 are close topological relatives is consistent with their abundance in random monodisperse foam.

Results for L, the total cell edge length per unit volume of foam, are presented in Table I. The data show that $L \approx 5.39$

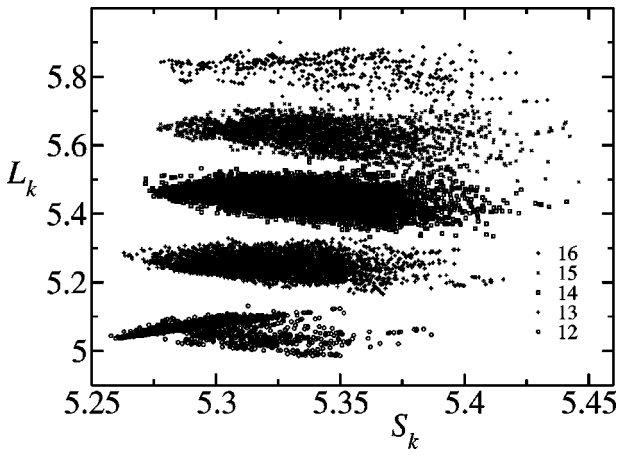

FIG. 11. Edge length L_k vs surface area S_k of individual cells in fully annealed foams.

for fully annealed foams and that L increases with E for all of the foams. The edge length L_k of individual foam cells is graphed against their surface area S_k and presented in Fig. 11. A cell with f faces has $3f$-6 edges. L_k is calculated by summing the edge lengths and dividing by three to compensate for the fact that each edge is shared by three cells. The figure shows that L_k is strongly correlated with f, in sharp contrast to S_k, which is not. L_k increases substantially with f even though each cell has the same volume. This is also illustrated in Fig. 12, which contains a graph of L_k vs n_4 (the number of quadrilateral faces on a cell) for different f. The edge length of f-hedra decreases slightly with n_4, which can be viewed as a measure of topological inhomogeneity. A cell has mostly pentagonal faces when $n_4=0$; it loses two pentagons and gains a hexagon with the addition of each quadrilateral.

The dependence of L_k on f and n_4 is captured by the following model. The surface area S_k of the kth cell can be expressed as

$$\begin{aligned} S_k &= n_4\langle\alpha_4\rangle + n_5\langle\alpha_5\rangle + n_6\langle\alpha_6\rangle \\ &= [n_4c_4 + (12-2n_4)c_5 + (f+n_4-12)c_6]\langle\lambda\rangle_k^2 \\ &= [c_6 f - 12(c_6-c_5) + (c_6-2c_5+c_4)n_4]\langle\lambda\rangle_k^2, \end{aligned} \quad (9)$$

where $\langle\alpha_n\rangle$ is the average area of a face with n sides, $\langle\lambda\rangle_k$ is the average edge length, and the geometric factors c_n are defined by $c_n=\langle\alpha_n\rangle/\langle\lambda\rangle_k^2$. All of these parameters refer to the kth cell. Equation (1) has been used to simplify Eq. (9). The edge length L_k per cell is given by

$$L_k = (f-2)\langle\lambda\rangle_k. \quad (10)$$

Combining Eqs. (9) and (10) gives

$$L_k = \frac{S_k^{1/2}(f-2)}{[c_6 f - 12(c_6-c_5) + (c_6-2c_5+c_4)n_4]^{1/2}}, \quad (11)$$

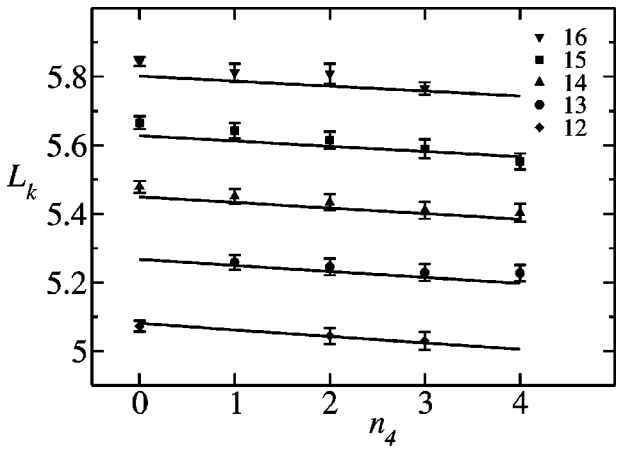

FIG. 12. Edge length L_k of individual *f*-hedra graphed against n_4, the number of quadrilateral faces they contain. The data represent several thousand cells from fully annealed foams. The curves refer to Eq. (11), which involves one adjustable parameter, $S_k = 5.33$.

which is exact if one allows the c_n and S_k to vary from cell to cell. We neglect this variation and let $S_k = 5.33$, the average cell area. The c_n are calculated by assuming that the faces are regular polygons:

$$c_n = \alpha_n / \lambda^2 = \frac{n}{4} \cot \pi / n. \tag{12}$$

The result is in excellent agreement with the data shown in Fig. 12.

The probability $p(\lambda)$ of finding an edge of length λ in the interval $\delta\lambda$ is shown in Fig. 13. Once again, there is a dramatic difference between Voronoi structures and relaxed foams. Voronoi partitions have very broad $p(\lambda)$ with many small edges and long edges; and V-RSA structures are the least foamlike. Fully relaxed foams have narrow $p(\lambda)$ and virtually no short edges. The average edge length is essentially constant, $0.430 \lesssim \langle \lambda \rangle \lesssim 0.460$; it is lower for V-RSA

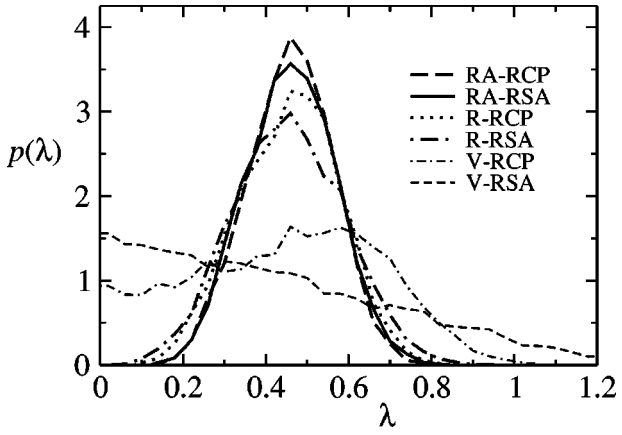

FIG. 13. Distribution of edge lengths in various foams with $N = 512$.

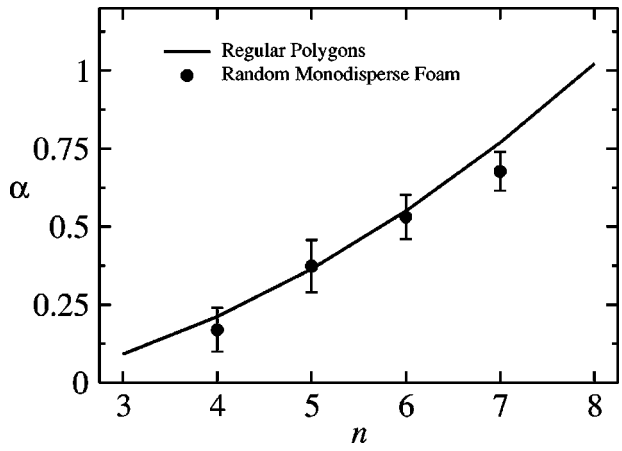

FIG. 14. The area α of faces with *n* edges compared against the area of regular polygons with edge length $\lambda = 0.46$ [see Eq. (12)].

foams and higher for fully annealed foams. The Kelvin foam (0.447) is in the middle of the range and Weaire-Phelan (0.465) is slightly higher.

The area α of a face tends to increase with the number of edges *n*. The results for a fully annealed foam presented in Fig. 14 are typical of all relaxed foams. The curve in Fig. 14 follows from Eq. (12) with $\lambda = 0.46$. This simple relation for the area of regular polygons captures the magnitude of α and the increase with *n*.

IV. CONCLUSIONS

The Surface Evolver was used to simulate the equilibrium microstructure of monodisperse soap froth that possesses topological disorder, a hallmark of real systems. The initial conditions are based on Voronoi tessellations, which in turn are based on random packings of identical spheres. Frequent topological transitions occur as the structure evolves toward some local minimum in surface free energy under the constraint that all of the cells have equal volume. The final energy and topological properties depend strongly on the initial state, which is controlled by the density of packed spheres. Loose packings ($\phi \approx 0.36$) were produced by random sequential adsorption and dense, random close packings ($\phi \approx 0.64$) were built with classical molecular dynamics techniques. The Voronoi structures that are based on RCP have smaller surface area and cell-volume dispersion, and evolve to equilibrium monodisperse foams with lower energy than their RSA counterparts. All Voronoi foams have $\langle f \rangle > 14$; all of the relaxed monodisperse foams have $\langle f \rangle \leqslant 14$. Ordered foams with $\langle f \rangle$ as large as 18 have been reported [49,50]. The random foams can be driven into lower energy minima with smaller $\langle f \rangle$ by annealing—subjecting them to large-deformation tension-compression cycles that involve step strains and relaxation. Persistent annealing achieves stationary states with $E = 5.330 \pm 0.006$ and $\langle f \rangle = 13.74 \pm 0.06$, but does not cause random foams to become ordered.

Matzke investigated bubble shapes in monodisperse foams that were assembled by sequentially depositing single bubbles onto the foam surface. The bubbles gained neighbors as they were being covered by other bubbles in the experi-

ment. In sharp contrast, Voronoi ''bubbles'' lose neighbors as the foams are relaxed and annealed in the computer. The experiments and simulations meet around $\langle f \rangle = 13.70$. Furthermore, the distribution of *f*-hedral cells and *n*-gonal faces, and the detailed census of cell types in experiment and simulation are in remarkable agreement. Matzke's results are upheld.

Random monodisperse foams with significantly different topological and geometric properties were simulated. The extent to which this diversity can be realized in real soap froth remains to be seen. Achieving and maintaining equal-volume bubbles and characterizing the foam structure while gas diffuses and liquid drains, is no less daunting a task today than half a century ago. Soap foams are fragile and far from true equilibrium.

We have investigated large systems, gathered meaningful statistics on foam topology, and calculated geometric properties related to surface area, edge length, and stress at the macroscopic level of the foam and microscopic level of the cells. The energy range for random monodisperse foam ($5.324 \lesssim E \lesssim 5.380$) slightly overlaps that of ordered foams ($5.2883 \leqslant E \leqslant 5.3421$).

Random spatially periodic foams (of finite size) confined to cubic unit cells do not have isotropic stress. Isotropy is achieved and surface area is reduced by relaxing the lattice. This procedure provides an estimate of the shear modulus that agrees with measurements by Princen and Kiss. Simple models based on regular polygons predict trends in the data for the edge length of individual cells and the area of individual faces.

We have introduced a new measure of shape anisotropy for individual cells, Q_k, which is related to the contribution of the faces to the foam stress. Graphs of surface area vs shape anisotropy reflect the geometrical frustration in foams. Pentagonal dodecahedra have lower surface area than other cells in monodisperse foams. The pentagonal dodecahedron and Matzke cell (1-10-2) are close relatives from a topological point of view. The latter becomes the former by losing a quadrilateral face. This shows why Matzke cells are so common—they aspire to become pentagonal dodecahedra so that they can reduce surface area.

The techniques presented here have been extended to investigate random polydisperse foams. Ongoing studies are providing a wealth of information on virtual foams that are very realistic [51].

ACKNOWLEDGMENTS

The authors would like to thank Ken Brakke for stimulating discussions, and for developing and maintaining the Surface Evolver. Gerry Seidler provided insightful comments on an early manuscript. Sandia is a multiprogram laboratory operated by Sandia Corporation, a Lockheed Martin Company, for the U.S. Department of Energy under Contract No. DE-AC04-94AL85000. This work was also supported by the Dow Chemical Company under a Cooperative Research and Development Agreement (CRADA).

[1] E.B. Matzke, Am. J. Botany **33**, 58 (1946).
[2] W. Thompson, Philos. Mag. **24**, 503 (1887).
[3] *The Kelvin Problem: Foam Structures of Minimal Surface Area*, edited by D. Weaire (Taylor and Francis, London, 1996).
[4] D. Weaire and R. Phelan, Philos. Mag. Lett. **69**, 107 (1994).
[5] T.C. Hales, Discrete Comput. Geom. **25**, 1 (2001).
[6] S. Perkowitz, *Universal Foam: From Cappuccino to the Cosmos* (Walker, New York, 2000).
[7] L.J. Gibson and M.F. Ashby, *Cellular Solids: Structure and Properties* (Cambridge University Press, Cambridge, 1997).
[8] *Foams and Emulsions*, Proceedings of the NATO Advanced Study Institute on Foams, Emulsions, and Cellular Materials, Cargese, France, 1997, edited by J.-F. Sadoc and N. Rivier (Kluwer Academic, Dordrecht, 1999).
[9] D. Weaire and S. Hutzler, *The Physics of Foam* (Oxford University Press, New York, 1999).
[10] S. Torquato, *Random Heterogeneous Materials: Microstructure and Macroscopic Properties* (Springer, New York, 2001).
[11] R. G. Larson, *The Structure and Rheology of Complex Fluids* (Oxford University Press, New York, 1999).
[12] *Jamming and Rheology: Constrained Dynamics on Microscopic and Macroscopic Scales* edited by A. J. Liu and S. R. Nagel, (Taylor and Francis, London, 2001).
[13] J.-F. Sadoc and R. Mosseri, *Geometrical Frustration* (Cambridge University Press, Cambridge, 1999).
[14] J. A. F. Plateau, *Statique Experimentale et Theorique des Liquides* (Gauthier-Villiard, Paris, 1873).
[15] J.E. Taylor, Ann. Math. **103**, 489 (1976).
[16] R.E. Williams, Science **161**, 276 (1968).
[17] N. Rivier, Philos. Mag. Lett. **69**, 297 (1994).
[18] F.C. Frank and J.S. Kasper, Acta Crystallogr. **12**, 483 (1959).
[19] J. M. Sullivan, in *Foams, Emulsions and their Applications*, Proceedings of the Third EuroConference on Foams, Emulsions and Applications (EuroFoam 2000), Delft, The Netherlands, 2000, edited by P. Zitha, J. Banhart, and G. Verbist, (Verlag MIT Publishing, Bremen, 2000), pp. 111–119.
[20] T. Aste and D. Weaire, *The Pursuit of Perfect Packing* (Institute of Physics, Bristol, 2000).
[21] J.-F. Sadoc and R. Mosseri, J. Phys. **46**, 1809 (1985).
[22] M. Hucher and J. Grolier, J. Microscopy **111**, 329 (1977).
[23] M. Hucher and J. Grolier, C.R. Acad. Sc. Paris **A284**, 219 (1977).
[24] C. Monnereau, B. Prunet-Foch, and M. Vignes-Adler, Phys. Rev. E **63**, 061402 (2001).
[25] K.A. Brakke, Exp. Math. **1**, 141 (1992).
[26] A.M. Kraynik, M.K. Neilsen, D.A. Reinelt, and W.E. Warren, in *Foams and Emulsions*, Proceedings of the NATO Advanced Study Institute on Foams, Emulsions, and Cellular Materials, Cargese, France, 1997, edited by J.-F. Sadoc, and N. Rivier, (Kluwer Academic, Dordrecht, 1999), pp. 259–286.
[27] D. Weaire and J.P. Kermode, Philos. Mag. B **48**, 245 (1983).
[28] L. Oger, A. Gervois, J.P. Troadec, and N. Rivier, Philos. Mag. B **47**, 177 (1996).
[29] P. Richard, J.P. Troadec, L. Oger, and A. Gervois, Phys. Rev. E **63**, 062401 (2001).

[30] R. Kusner and J. M. Sullivan, in *The Kelvin Problem: Foam Structures of Minimal Surface Area*, edited by D. Weaire (Taylor and Francis, London, 1996), pp. 71–80.
[31] R. Kusner and J.M. Sullivan, Forma **11**, 233 (1996).
[32] K.A. Brakke, *The Motion of a Surface by Its Mean Curvature* (Princeton University Press, Princeton, 1977).
[33] The Surface Evolver has been developed, maintained, and freely distributed by Ken Brakke. It is available at http://www.susqu.edu/facstaff/b/brakke/evolver/
[34] H.W. Schwarz, Recueil **84**, 771 (1964).
[35] M.A. Fortes and A.C. Ferro, Acta Metall. **33**, 1697 (1985).
[36] D.A. Reinelt and A.M. Kraynik, J. Rheol. **44**, 453 (2000).
[37] A.M. Kraynik and D.A. Reinelt, Forma **11**, 255 (1996).
[38] D.A. Reinelt and A.M. Kraynik, J. Fluid Mech. **311**, 327 (1996).
[39] A.D. Gopal and D.J. Durian, Phys. Rev. Lett. **75**, 2610 (1995).
[40] A.D. Gopal and D.J. Durian, J. Colloid Interface Sci. **213**, 169 (1999).
[41] G.K. Batchelor, J. Fluid Mech. **41**, 545 (1970).
[42] G. K. Batchelor, *An Introduction to Fluid Dynamics* (Cambridge University Press, Cambridge, 1970).
[43] M. Doi and T. Ohta, J. Chem. Phys. **95**, 1242 (1991).
[44] K. Kendall, C. Stainton, F. van Swol, and L.V. Woodcock, Int. J. Thermophys. **23**, 175 (2002).
[45] A.M. Kraynik and D.A. Reinelt, J. Colloid Interface Sci. **181**, 511 (1996).
[46] H.M. Princen and A.D. Kiss, J. Colloid Interface Sci. **112**, 427 (1986).
[47] H. M. Princen, in *Encyclopedic Handbook of Emulsion Technology*, edited by J. Sjoblom (Marcel Dekker, New York, 2001), pp. 243–278.
[48] K. A. Brakke (private communication).
[49] M. O'Keeffe and J.M. Sullivan, Z. Kristallogr. **213**, 374 (1998).
[50] J. M. Sullivan (private communication).
[51] S. Hilgenfeldt, A.M. Kraynik, S.A. Koehler, and H.A. Stone, Phys. Rev. Lett. **86**, 2685 (2001).